Electrochemical microfluidic immunosensor based on TES-AuNPs@Fe_3O_4 and CMK-8 for IgG anti-*Toxocara canis* determination

Claudio F. Jofre[a], Matías Regiart[b], Martin A. Fernández-Baldo[a], Mauro Bertotti[b], Julio Raba[a], Germán A. Messina[a,*]

[a] *INQUISAL. Department of Chemistry, National University of San Luis. CONICET. Chacabuco 917. D5700BWS. San Luis, Argentina.*

[b] *Department of Fundamental Chemistry, Institute of Chemistry, University of São Paulo, Av. Prof. Lineu Prestes, 748, 05508-000 São Paulo, SP, Brazil.*

Authors to whom correspondence should be addressed: *Germán A. Messina (messina@unsl.edu.ar) (Tel.) +54 266 442 5385; (Fax) +54 266 443 0224. INQUISAL. Departamento de Química, Universidad Nacional de San Luis. CONICET. Chacabuco 917. D5700BWS. San Luis, Argentina.

Abstract

We report a microfluidic immunosensor for the electrochemical determination of IgG antibodies anti-*Toxocara canis* (IgG anti-*T. canis*). In order to improve the selectivity and sensitivity of the sensor, core-shell gold-ferric oxide nanoparticles (AuNPs@Fe_3O_4), and ordered mesoporous carbon (CMK-8) in chitosan (CH) were used. IgG anti-*T. canis* antibodies detection was carried out using a non-competitive immunoassay, in which excretory secretory antigens from *T. canis* second-stage larvae (TES) were covalently immobilized on AuNPs@Fe_3O_4. CMK-8-CH and AuNPs@Fe_3O_4 were characterized by transmission electron microscopy, scanning electron microscopy, energy dispersive spectrometry, cyclic voltammetry, electrochemical impedance spectroscopy, and N_2 adsorption-desorption isotherms.

Antibodies present in serum samples immunologically reacted with TES, and then were quantified by using a second antibody labeled with horseradish peroxidase (HRP-anti-IgG). HRP catalyzes the reduction from H_2O_2 to H_2O with the subsequent oxidation of catechol (H2Q) to p-benzoquinone (Q). The enzymatic product was detected electrochemically at −100 mV on a modified sputtered gold electrode. The detection limit was 0.10 ng mL^{-1}, and the coefficients of intra- and inter-assay variation were less than 6 %, with a total assay time of 20 min. As can be seen, the electrochemical immunosensor is a useful tool for in situ IgG antibodies anti-*T. canis* determination.

Keywords: *Toxocara canis*; Toxocariosis; AuNPs@Fe_3O_4; Microfluidic immunosensor; Electrochemical.

1. Introduction

Toxocariosis is a disease caused by *Toxocara canis* and less commonly by *Toxocara cati*, which are global prolific nematodes with a complex life cycle [1]. The infection in humans is acquired by oral route through accidental ingestion of infective eggs from soil-contaminated hands, consumption of poorly sanitized vegetables, and uncooked meats [2, 3]. *Toxocara* eggs hatch in the intestine and release larvae into the lumen, where they can penetrate the intestine, reach the circulation and then spread by the systemic route. The larvae migrate throughout the body but cannot mature, and instead encyst as second-stage larvae [4]. The inflammatory process, caused by the larvae stage, is attributed to small amounts of secretion and excretion products (lectins, mucins, enzymes), which interact and modulate the host immune response [5]. In brief, clinical manifestations of toxocariosis are related to the larval migration and the host immune response. The clinical forms of toxocariosis are systemic (visceral larva migrans), localized (ocular and neurological), and asymptomatic [6].

Human toxocariosis is diagnosed by clinical manifestations, ophthalmology (OLM), clinical pathology, including eosinophilia, bioimaging, and serology. In cases of OLM, extirpation by biopsy and subsequent histopathology can be performed and parasite material can be speciated by PCR. Moreover, serological methods using immunological techniques are recognized as the most effective approach to the laboratory diagnosis of human toxocariosis [7]. In this context, detection of IgG antibodies to *T. canis* by methods as enzyme-linked immunosorbent assay (ELISA) using excretory-secretory antigens from *T. canis* second stage larvae (TES) is the most widely used [8, 9].

In recent years, immunosensors promise to be the solution to the immunodiagnostic of various parasitic diseases [10-15]. In addition, microfluidic immunosensors with

electrochemical detection represent an attractive strategy due to their advantages, such as the high degree of integration, low consumption of reagents and samples, and low detection limit [16-18]. These devices are considered to be valuable and promising due to their robustness, simplicity, sensitivity, ease of handling, cost-effectiveness, rapid analysis and miniaturization ability [19, 20]. Furthermore, microfluidic immunosensors modified with nanoparticles possess higher selectivity than naked sensors, and have higher sensitivity because of the increased surface area provided by the nanoparticles [21-24**]**. Recently, the synthesis of magnetic nanoparticles increased, and they were applied in numerous scientific fields such as proteins purification, biological separations, target delivery, magnetic resonance imaging, therapy, and biosensors fabrication [25-27]. In addition, much interest has been deposited in the incorporation of magnetic nanomaterials to other functional platforms or nanostructures. The exceptional applicability properties are the advantages of the new structures [28]. Among these, the iron-gold core-shell structure has drawn attention due to the apparent benefits of gold nanoparticles (AuNPs). Gold is an inert element, very useful as a coating material for protecting magnetic nanoparticles, due to the high versatility in surface modification processes, great catalytic properties, and unique biocompatibility [29, 30]. Up till now, gold-ferric oxide core/shell nanoparticles (AuNPs@Fe_3O_4) have been considered as excellent candidates to be used as biomolecules immobilization platform, for capture and recognition elements (antigens, antibodies, enzymes or DNA) in microfluidic immunosensors, because of their simple synthesis, excellent biocompatibility and large surface area [31].

Another strategy to be employed in the microfluidic immunosensor design is the modification of the working electrode surface with different materials, such as ordered mesoporous carbons (OMCs) [32]. OMCs like CMK-8 have been used for electrode

modification because of their excellent electrical conductivity, high surface area, chemical and thermal stability, and their facile functionalization [33-36].

In the present work, we developed an electrochemical microfluidic immunosensor for the toxocariosis diagnosis based on the use of core-shell AuNPs@Fe_3O_4 for covalent immobilization of TES antigen, and the working electrode modification with CMK-8 in chitosan (CH). IgG anti-*T. canis* antibodies present in the serum samples were detected by using a non-competitive immunoassay into the microfluidic device. To the best of our knowledge, this is the first electrochemical microfluidic immunosensor reported for the IgG anti-*T. canis* antibodies detection based on magnetic core-shell nanoparticles and ordered mesoporous carbon materials.

2. Experimental

2.1. Materials and reagents

All reagents used were of analytical reagent grade. Triblock copolymer P123, tetraethyl orthosilicate (TEOS 98%), CH (from crab shells, medium molecular, 85% deacetylated), $FeCl_2$, $FeCl_3$, $[Fe(CN)_6]^{3-/4-}$, $HAuCl_4$, 3-mercaptopropionic acid (MPA), Bovine serum albumin (BSA), 4-tert-butylcatechol (4-TBC) N-(3-dimethylaminopropyl)-N-ethylcarbodiimide (ECD), and N-hydroxysuccinimide (NHS) were acquired from Sigma-Aldrich, St. Louis, USA. Disodium phosphate (Na_2HPO_4), monosodium phosphate (NaH_2PO_4), trisodium citrate dehydrate, potassium chloride (KCl), and ethanol were purchased from Merck (Darmstadt, Germany). SU-8 photoresist, Sylgard 184, including PDMS prepolymer and curing agent were obtained from Clariant Corporation (Sommerville, NJ, USA) and Dow Corning (Midland, MI, USA), respectively. The enzyme immunoassay for the qualitative determination of IgG antibodies against Toxocara canis in

human serum (RIDASCREEN® Toxocara IgG test) was purchased from R-Biopharm AG (Darmstadt, Germany), and used according to the manufacturer's instructions. Anti-human γ-chain was purchased from Abcam (USA). All the other employed reagents were of analytical grade and were used without further purification. Aqueous solutions were prepared by using purified water from a Milli-Q system.

2.2. Apparatus

Amperometric and voltammetric experiments were performed with a BAS LC-4C Electrochemical Detector, and a BAS 100 B/W Electrochemical Workstation (Bioanalytical Systems, Inc. West Lafayette, IN, USA), respectively. Electrochemical measurements were carried out using a microfabricated electrochemical cell with three electrodes (gold working and counter electrodes, and silver reference electrode). All the potentials were referred to Ag. EIS measurements were performed using a PGSTAT128N potentiostat from Methrohm Autolab, with a NOVA 1.11 electrochemical analysis software.

Scanning electron microscope images were taken on a LEO 1450VP instrument (UK), equipped with an Energy Dispersive Spectrometer analyzer, Genesis 2000 (England). Sputtering deposition was made with a SPI-Module Sputter Coater (Structure Probe Inc, West Chester, PA). The electrode thickness was controlled using a Quartz Crystal Thickness Monitor model 12161 (SPI-Module, Structure Probe Inc, West Chester, PA).

A syringe pumps system (Baby Bee Syringe Pump, Bioanalytical Systems, Inc. West Lafayette, IN, USA) was used for introducing the solutions in the device. All solutions employed were injected using syringe pumps at flow rate of 2 μL min^{-1}. All solutions and reagent temperatures were conditioned before the experiment using a Vicking Masson II laboratory water bath (Vicking SRL, Buenos Aires, Argentina). Absorbance was

detected by Bio-Rad Benchmark microplate reader (Japan) and Beckman DU 520 general UV/VIS spectrophotometer. All pH measurements were made with an Orion Expandable Ion Analyzer (Orion Research Inc., Cambridge, MA, USA) Model EA 940 equipped with a glass combination electrode (Orion Research Inc).

2.3. Fabrication of the microfluidic device

The microfluidic device manufacture involved four steps: i) Deposition of Ag/Au electrodes by sputtering on a glass plate, ii) Fabrication of the PMDS molds by photolithography, iii) CMK-8-CH deposition on the Au working electrode (GE), and iv) Sealing of the glass/PDMS. The fabrication of the microfluidic electrochemical immunosensor was carried out according to the procedure previously reported with the following modifications [18] (Scheme 1): For the construction of the electrode, a self-adhesive vinyl sheet patterned mask was employed. The mask was positioned at the end of the central channel (CC), followed by sputtering deposition of 100 nm silver and 100 nm gold over a glass plate. The vinyl mask was removed after sputtering, leaving the gold and silver tracks on the glass. The geometric area was 1.0 mm^2 for the working electrode, and 2.0 mm^2 for the counter and reference electrodes.

PDMS microchannels were cast by photolithography. The channels design in the negative mask was generated by a computer program. The replication master was patterned with a SU-8 photoresist layer over a silicon wafer using a spin coater at 2200 rpm for 30 s, and baked at 60 °C for 2 min and 90 °C for 5 min. Then, the coated sheet was exposed to a UV lamp through a negative mask with the T-configuration design (two inlets for reagents and buffer, respectively and one outlet) with 200-μm-width and 100-μm-hight, with a central channel (CC) (40 mm length, 200-μm-width, and 100-μm-hight). After that, the

unexposed photoresist was removed. Then, the Sylgard curing agent was mixed with PDMS prepolymer (1:10), and placed on the replication master (degassed for 30 min to eliminate air bubbles). The polymer curing process was carried out in a hot plate at 70 °C for 45 h. The PDMS was then peeling off, and the external access to the microfluidic device was obtained by drilling holes. After that, the glass plate and PDMS were placed in oxygen plasma for 1 min and were contacted immediately for a strong seal.

2.4. Synthesis of CMK-8

As mentioned before, CMK-8 was prepared using KIT-6 as a hard template. KIT-6 was synthetized according to a procedure previously reported with slight modifications [37]. Firstly, 9.6g:346.6g:18.8g of P123, double distilled water and HCl, respectively, were mixed. After P123 dissolution, 9.6 g of butanol were added, and the solution was stirred for 1 h at 35 °C, followed by addition of 24.8 g TEOS with continuous stirring at 35 °C for 12 h. Then, the temperature was raised at 120 °C for 24 h. The white precipitate was washed by double distilled water several times, and dried at 120 °C. KIT-6 was obtained after calcination at 550 °C for 3 h.

CMK-8 was synthesized following the procedure with some modifications [36]. Sucrose was used as a carbon source. Firstly, 0.5g:0.6g:0.1g:5mL KIT-6, sucrose, H_2SO_4 and H_2O were mixed and stirred for 15 min. Then, the suspension was dried at 100 °C for 6 h, followed by increasing the temperature at 160 °C for another 6 h. After that, a second impregnation step was carried out to ensure the KIT-6 pores filling by adding 2mL:0.4g:0.05g H_2O, sucrose and H_2SO_4, followed by the temperature treatment. The dark brown mixture was carbonized at 900 °C in N_2 for 6 h to achieve complete carbonization. Lastly, the powder was washed several times with 2 mol L^{-1} NaOH in order to remove the

inorganic silica template. The black solid was filtered and washed with ethanol:NaOH (50:50 % v/v), and finally dried at 120 °C for 12 h.

In order to improve the hydrophilicity of mesoporous carbon for the electrochemical use in sensors, CMK-8 was treated with 70 % HNO_3 at 60 °C for 1 h and subsequently washed with double distilled water until neutral pH [34]. CMK-8 was characterized by transmission electron microscopy (TEM), and N_2 adsorption-desorption isotherms.

2.5. CMK-8-CH/GE preparation

A chitosan solution was prepared by adding 1 g of CH in 100 mL of an ethanol:H_2O (1:4) mixture at pH 3.00 with HCl addition under stirring conditions. The undissolved material was filtered. Then, the pH value was gradually increased to 8.00 with NaOH. 1 % CH solution was stored at 4 ºC until use [38].

After that, 0.9 mg of CMK-8 was dispersed in 1 mL of 1 % CH with the ultrasonic stirring aid for 1 h. The CMK-8-CH suspension was stable for at least 2 months at 4 ºC. Finally, 10 µL of the obtained CMK-8-CH were dropped on the GE, and the solvent was evaporated under an infrared heat lamp. CMK-8-CH/GE was characterized by scanning electron microscopy (SEM), energy dispersive spectrometry (EDS), cyclic voltammetry (CV), and electrochemical impedance spectroscopy (EIS).

2.6. Synthesis of core-shell AuNPs@Fe_3O_4

Firstly, Fe_3O_4 nanoparticles were prepared by co-precipitation method following the procedure previously published by Salihov et al. with some modifications [29]. Briefly, a 100 mL 0.1 mol L^{-1} $FeCl_2$·and 0.2 mol L^{-1} $FeCl_3$ solution was prepared with 0.1 mol L^{-1} HCl. Then, 1 mol L^{-1} NaOH was added dropwise under stirring condition at 75 °C for 50

min under N_2 atmosphere. The black suspension obtained was separated using a neodymium magnet, and washed several times using N_2 purged double distilled water. The Fe_3O_4 nanoparticles suspension was dried in vacuum oven and kept at 4 °C for further use.

After that, Fe_3O_4 nanoparticles were resuspended in double distilled water, and the suspension was ultrasonicated for 15 min. Then, 1 mL of 0.1 mol L^{-1} $HAuCl_4$ solution was added to the suspension in stirring condition at 75 °C. Finally, 5 mL of 0.1 mol L^{-1} trisodium citrate dehydrate solution were added to the mixture [39]. The solution was stirred at 75 °C for 45 min until a reddish color suspension. AuNPs@Fe_3O_4 nanoparticles were washed several times using N_2 purged double distilled water using a neodymium magnet. The suspension was dried in vacuum oven and kept at 4 °C for further use. AuNPs@Fe_3O_4 was characterized by SEM and EDS.

2.7. *T. canis* second-stage larvae (TES) antigen preparation

TES antigens were obtained according to the technique described by Gillespie [13]. TES were maintained at 35 °C with 5 % CO_2 atmosphere and adjusted to pH 6.5 in Iscove's modified Dulbecco's culture medium supplemented with HEPES buffer and a Penicillin-Streptomycin solution. The culture supernatant was removed weekly, and the supernatant pool was kept at -70 °C. The supernatant pool was concentrated by filtration through polyethersulphone membranes and dialysed. The protein content was then estimated by the Bradford method with bovine albumin as the standard protein.

2.8. TES immobilization on AuNPs@Fe_3O_4

10 mg of AuNPs@Fe_3O_4 were resuspended with MPA 50 mmol L^{-1} in an EtOH:H_2O (75:25, v/v) mixture for 12 h at 25 ºC. The thiol group of MPA reacts with the

Au surface, giving, as a result, free carboxylic groups, which are activated by rinsing with an EDC:NHS solution in 10 mmol L^{-1} phosphate buffer saline (PBS) for 2 h at pH 7.00. Then, the AuNPs@Fe_3O_4 nanoparticles were washed several times using a neodymium magnet and dried with N_2.

After that, the AuNPs@Fe_3O_4 were put in contact with 1 mL of 100 μg mL^{-1} TES solution in 10 mmol L^{-1} PBS pH 7.00 for 10 h at 4 ºC. Finally, the nanoparticles were rinsed with 10 mmol L^{-1} PBS pH 7.00 and stored in the same buffer at 4 ºC when not in use. The immobilized antigen preparation was perfectly stable for at least 1 month. Scheme 2 shows the procedure for TES-AuNPs@Fe_3O_4 preparation.

2.9. Analytical procedure for anti-*T. canis* IgG antibodies determination

In this work, six serum samples obtained from patients with toxocariasis were analyzed. These samples showed a marked reactivity against *T. canis.* The procedure for anti-*T. canis* IgG antibodies determination involves the following steps. Firstly, TES-AuNPs@Fe3O4 was introduced into the microfluidic channel and kept in the central channel using an external neodymium magnet. To avoid the unspecific bindings, a blocking treatment was carried out through with 1 % of bovine serum albumin (BSA) in 10 mmol L^{-1} PBS pH 7.00 for 5 min, followed by a washing step with 10 mmol L^{-1} PBS pH 7.00 for 2 min.

Then, the serum samples (previously diluted 50-fold with 10 mmol L^{-1} PBS pH 7.00), were injected for 5 min, followed by the washing step to remove the excess of the sample. In this step, the IgG specific antibodies to *T. canis* present in the samples react with TES immobilized on AuNPs@Fe3O4 surface. Later, IgG anti-*T. canis* were quantified by using a second antibody labeled with horseradish peroxidase (HRP-anti-IgG). HRP

catalyzes the reduction of H_2O_2 to H_2O, with the subsequent oxidation of catechol (H2Q) to p-benzoquinone (Q). Finally, the substrate solution (1 mmol L^{-1} H_2O_2 + 1 mmol L^{-1} 4-TBC in 10 mmol L^{-1} phosphate-citrate buffer pH 5.00) was pumped, and the enzymatic product was detected by amperometry at -100 mV in the CMK-8-CH/GE (Scheme 2).

Before each sample analysis, the immunosensor was exposed to a desorption buffer (0.1 mol L^{-1} citrate-HCl pH 2.00) for 5 min and then washed with 10 mmol L^{-1} PBS pH 7.00. This procedure desorbed the anti-*T. canis* antibodies bound to immobilized TES, allowing to performed a new determination. The device can be used without significant loss of sensitivity for 1 month (decrease of 10 %). The microfluidic immunosensor was stored in 10 mmol L^{-1} PBS pH 7.00 at 4 ºC.

3. Results and discussion

3.1. CMK-8-CH/Au and AuNPs@Fe_3O_4 characterization

CMK-8 specific surface area (SBET) was calculated according to the Brunauer-Emmet-Teller method, using the adsorption data at relative pressures. Total pore volume (VTP) was found by the Gurvich's rule. CMK-8 pore size distribution (PSD) was determined by VBS macroscopic method using the adsorption branch data [38]. Figure 1 a) shows a TEM image of CMK-8. The micrograph reveals a uniform long-range ordered mesoporous cubic pore structure with a 10 nm pore size approximately. Also, a study on the N_2 adsorption-desorption isotherm at 77 K was carried out, and a type IV isotherm with an H2 hysteresis loop characteristic of mesoporous materials can be clearly seen (Figure 1 b). CMK-8 textural properties, obtained from adsorption data, were SBET: 817 m^2 g^{-1}, and VTP: 0.7 cm^3 g^{-1}. Figure 1 b) (inset), confirming that CMK-8 has a narrow pore size distribution around 9 nm.

Morphology of the CMK-8-CH/GE nanocomposite film was analyzed by SEM. Figure 1 c) reveals a uniform CMK-8-CH film over the gold electrode surface. The nanocomposite three-dimensional structure film provides a suitable surface for a conductive pathway for electron-transfer. The nanocomposite elemental composition was determined by EDS. Figure 1 d) shows five peaks, corresponding to C, O, Si, Au, and Ag elements, respectively.

CV of $[Fe(CN)_6]^{3-/4-}$ couple is an appropriate tool to study the electrode surface properties during several modification steps. Accordingly, Figure 2 a) shows CVs recorded with a bare GE and the CMK-8-CH/GE. Well-defined CVs characteristics of a diffusion-controlled redox process were perceived at the bare GE, whereas enlarged peaks were noticed with the electrode modified with CMK-8-CH. The higher faradaic response observed with the CMK-8-CH/GE can be attributed to the increased electroactive surface area, and the excellent electrical conductivity of CMK-8. Another factor to take account is the hydrophilic surface obtained due to the synergic effect between CMK-8 and chitosan, which allow to improve the solution/electrode contact.

Electrochemical impedance spectroscopy was recorded in 5 mmol L^{-1} $[Fe(CN)_6]^{4-/3-}$ in 0.1 mol L^{-1} KCl, applying a +150 mV potential and varying the frequency with logarithmic spacing frequency in the range from 0.1 Hz to 100 kHz. EIS data were represented in Nyquist plots (Fig. 2 b)), where the impedance spectrums includes a semicircle at higher frequencies that represents the electron transfer resistance (evidencing the blocking behavior of the bare/modified electrode surface towards the redox couple), and a linear part at lower frequencies that represents the diffusion process. The analytical signal considered is the R_{ct}, evaluated by the iterative fitting of the experimental data to the modified Randles equivalent circuit (Fig. 2 b), inset), where R_s is the solution resistance, Z_w

is the Warburg impedance, and CPE is the constant phase element. As can be observed, the bare GE displays a lower electron transfer resistance (69 Ω), and the semicircle increased (R_{ct}= 143 Ω) for the CH/GE due to the presence of an insulating layer formed as a consequence of the CH polymer deposition process. Such partial blockage of the electron transfer is then alleviated for the CMK-8-CH/GE, because of the excellent electrical conductivity of CMK-8, hence a decrease in the semicircle curve (Rct= 19 Ω) was noticed.

As shown in Figure 2 c), a linear relationship between redox peak current and the square root of the scan rate is established in the 25 to 200 mV s^{-1}range, indicating the electron-transfer process is diffusion controlled for the CMK-8-CH/GE. The apparent electroactive surface area of this modified electrode can be calculated by the Randles-Sevcik equation and the value was found to be 0.195 cm^2.

Regarding the AuNPs@Fe_3O_4 nanoparticles characterization, Figure 3 a) shows the SEM images, and the nanoparticles diameters ranged from 10 to 50 nm. The nanoparticles elemental composition was determined by EDS and the O, Fe, and Au typical peaks can be clearly seen (Figure 3 b)).

3.2. Optimization of experimental parameters

Experimental parameters that affect the IgG anti-*T. canis* quantitation in biological samples were studied. For this purpose, an anti-*T. canis* IgG standard solution of 40 ng mL^{-1} was employed.

Firstly, the optimal flow rate for samples and reagents was analyzed employing several flow rates and evaluating the generated current during the immune reaction. As shown in Figure 4 a), flow rates varied from 1 to 2.5 μL min^{-1}, showing an increase in the current response with the flow rate until 2.5 μL min^{-1}. Then, the signal decreased slightly

due to the high flow reduced the interaction time between the immune reagents. Therefore, a flow rate of 2 μL min^{-1} was used for reagents, samples, and washing solutions.

The influence of pH on the enzymatic response under flow conditions was also examined in the range from 4.00 to 6.50 (Figure 4 b). A current increase until pH 5.00 can be observed followed by a decrease at higher pH values up to pH 6.50. So, the pH 5.00 was selected as optimum in 10 mmol L^{-1} phosphate-citrate buffer.

CMK-8 concentration employed for the gold electrode surface modification was also optimized. This study was carried out in the 0.5 to 1.2 mg mL^{-1} range. A significant signal increase was observed from 0.5 to 0.9 mg mL^{-1}. However, at higher concentrations, insignificant differences were obtained. Then, 0.9 mg mL^{-1} CMK-8 was employed for the modification step (Figure 4 c)).

An important parameter to be optimized was the concentration of the *T. canis* second-stage larvae (TES) to be immobilized in the AuNPs@Fe_3O_4. Such study was performed from 10 to 125 μg mL^{-1} TES, and the current response increased until 100 μg mL^{-1} TES. No significant changes were observed for higher TES concentrations, hence 100 μg mL^{-1} TES was employed as an optimum concentration for AuNPs@Fe_3O_4 immobilization (Figure 4 d)).

Other important parameters such as CH concentration, amount of AuNPs@Fe_3O_4 nanoparticles, among others, were also optimized (Data not shown).

3.4. Analytical performance of the microfluidic immunosensor

The analytical performance of our immunosensor was studied by measuring the response towards varying concentrations of anti-*T. canis* IgG in the 0.1-100 ng mL^{-1} concentration range. A linear relationship was observed between 0.33-75 ng mL^{-1}. The

calibration curve was obtained by plotting current (nA) versus anti-*T. canis* IgG concentration (ng mL^{-1}). The calibration curve was defined by ΔI (nA) = 15.86 – 2.21 $C_{T. canis}$ with a correlation coefficient of 0.992, where ΔI is the difference between blank and sample current. The standard deviation (SD) for the calibration curve was 4.45. The coefficient of variation (CV) for the determination of 40 ng mL^{-1} anti-*T. canis* IgG was below 4.92% (n=5). These values demonstrate that our microfluidic electrochemical immunosensor can be used to anti-*T. canis* IgG quantification in unknown samples. The limit of detection (LD) and the limit of quantification (LQ) were calculated according the IUPAC recommendations. For the electrochemical detection procedure, the LD and LQ were 0.10 and 0.5 ng mL^{-1}, respectively.

The precision of the electrochemical assay was checked with six anti-*T. canis* IgG standard solutions. The within-assay precision was tested with five measurements on the same day. These analyses were repeated for three consecutive days in order to estimate between-assay precision. The assay showed excellent precision; the CV % within-assay values were below 5 %, and the between-assay values were below 6 % (Table 1). The total assay time for anti-*T. canis* IgG determination was 20 min, much less than the time generally used for the conventional ELISA.

The electrochemical method was compared with the fluorescent immunosensor previously reported, where IgG anti-*T. canis* was quantified using 3-aminopropyl-functionalized silica-nanoparticles (AP-SNs) and cadmium selenide zinc sulfide quantum dots (CdSe-ZnS QDs) [13]. The slope obtained was practically close to the unit, indicating a good correspondence between both methods. Compared with the fluorescent immunosensor, the electrochemical immunosensor showed an improved LD. The F-test value for the immunosensor was 0.43 (the F-test value is 2.26 at a 95 % confidence level).

In order to evaluate the analytical applicability of the electrochemical immunosensor, IgG anti-*Toxocara canis* quantification was carried out in six human serum samples with toxocariasis, under the conditions previously described. These samples were confirmed by fluorescent immunosensor and commercial ELISA. The samples analyzed revealed similar IgG anti-*T. canis* concentrations, as can be observed in Table 2.

4. Conclusions

The designed microfluidic electrochemical immunosensor for IgG anti-*T. canis* detection in human serum samples shows outstanding analytical parameters. Our analytical method is based on the covalently immobilization of *T. canis* second-stage larvae antigens on core-shell gold nanoparticles-ferric oxide (AuNPs@Fe_3O_4) retained by an external magnet in the microfluidic channel. IgG anti-*T. canis* antibodies detection was carried out using a non-competitive immunoassay. The enzyme electrochemical mediator was measured over the order mesoporous carbon-chitosan (CMK-8-CH) modified gold electrode. The synthesized CMK-8 showed high specific surface area, large pore volume, uniform mesostructure, good conductivity, and excellent electrochemical activity, that allowed us to greatly improve the surface area of the sensor and its analytical performance.

The total assay time employed was shorter than the time reported for commercial ELISA frequently used. The microfluidic electrochemical immunosensor offered several attractive advantages like high stability, high selectivity, and sensitivity. In conclusion, the device could be well suitable for biomedical sensing and clinical applications for diagnosis and prognosis of toxocariosis in serum human samples.

Acknowledgements

The authors wish to thank the financial support from the Universidad Nacional de San Luis (PROICO-1512-22/Q232), the Agencia Nacional de Promoción Científica y Tecnológica, the Consejo Nacional de Investigaciones Científicas y Técnicas (CONICET) (PICT-2015-2246, PICT 2015-3526, PICT-2015-1575, PICT-2014-1184, PICT-2013-3092, PICT-2013-2407), and Fundação de Amparo à Pesquisa do Estado de São Paulo (FAPESP) (2019/06293-6).

References

[1] P. Nejsum, M. Betson, R.P. Bendall, S.M. Thamsborg, J.R. Stothard, Assessing the zoonotic potential of *Ascaris suum* and *Trichuris suis*: looking to the future from an analysis of the past, J. Helminthol. 86 (2012) 148-155.

[2] D. Choi, J. Lim, D. Choi, S. Paik, S. Kim, S. Choi, Toxocariasis and ingestion of raw cow liver in patients with eosinophilia, Korean J. Parasitol. 46 (2008) 139-143.

[3] S. Archelli, G. Santillan, R. Fonrouge, G. Céspedes, L. Burgos, N. Radman, Toxocariasis: seroprevalence in abandoned institutionalized children and infants, Rev. Argent. Microbiol. 46 (2014) 3-6.

[4] A.J. Cassenote, A.R. de Abreu Lima, J.M. Pinto Neto, G. Rubinsky-Elefant, Seroprevalence and modifiable risk factors for Toxocara spp. in Brazilian schoolchildren, PLoS. Neglect. Trop. D. 8 (2014) 2830.

[5] L.R. Mendonca, R.V Veiga, V.C.C Dattoli, C.A. Figueiredo, R. Fiaccone, J. Santos, A.A. Cruz, L.C. Rodrigues, P.J. Cooper, L.C. Pontes-de-Carvalho, M.L. Barreto, N.M. Alcantara-Neves, Toxocara seropositivity, atopy and wheezing in children living in poor neighbourhoods in urban Latin American, PLoS. Neglect. Trop. D. 6 (2012) 1886.

[6] E.V. Guilherme, A.A. Marchioro, S.M. Araujo, D.L. Falavigna, C. Adami, G. Falavigna-Guilherme, G. Rubinsky-Elefant, A.L. Falavigna-Guilherme, Toxocariasis in children attending a public health service pneumology unit in Parana State, Brazil, Rev. Inst. Med. Trop. 55 (2013) 189-192.

[7] J.K. Magnaval, L. Glickman, P. Dorchies, B. Morassin, Highlights of human Toxocariasis, Korean J. Parasitol. 39 (2001) 1-11.

[8] J. Fillaux, J.F. Magnaval, Laboratory diagnosis of human toxocariasis, Vet. Parasitol. 193 (2013) 327-336.

[9] H. Smith, C. Holland, M. Taylor, J.F. Magnaval, P. Schantz, Maizels R. How common is human toxocariasis? Towards standardizing our knowledge. Trends. Parasitol. 25 (2009) 182-188.

[10] I.C. Prado, V.G. Mendes, A.L.A. Souza, R.F. Dutra, S.G. De-Simone, Electrochemical immunosensor for differential diagnostic of Wuchereria bancrofti using a synthetic peptide, Biosens. Bioelectron. 113 (2018) 9-15.

[11] J. Ramos-Jesus, L.C. Pontes-de-Carvalho, S.M. Barrouin Melo, N.M. Alcântara-Neves, R.F. Dutra, A gold nanoparticle piezoelectric immunosensor using a recombinant antigen for detecting Leishmania infantum antibodies in canine serum, Biochem. Eng. J. 110 (2016) 43-50.

[12] S.V. Pereira, F.A. Bertolino, M.A. Fernández-Baldo, G.A. Messina, E. Salinas, M.I. Sanz, J. Raba, Microfluidic device based on a screen-printed carbon electrode with electrodeposited gold nanoparticles for the detection of IgG anti-*Trypanosoma cruzi* antibodies, Analyst. 136 (2011) 4745-4751.

[13] V. Medawar, G.A. Messina, M.A. Fernández Baldo, J. Raba, S.V. Pereira, Fluorescent immunosensor using AP-SNs and QDs for quantitation of IgG anti-*Toxocara cani*s, Microchem. J. 130 (2017) 436-441.

[14] Serological diagnosis of Toxoplasmosis disease using a fluorescent immunosensor with chitosan-ZnO-nanoparticles, V. Medawar-Aguilar, C.F. Jofre, M.A. Fernández-Baldo, A. Alonso, S. Angel, J. Raba, S.V. Pereira, G.A. Messina, Anal. Biochem. 564-565 (2019) 116-122.

[15] E.A. Takara, S.V. Pereira, M.L. Scala-Benuzzi, M.A. Fernández-Baldo, J. Raba, G.A. Messina, Novel electrochemical sensing platform based on a nanocomposite of PVA /

PVP / RGO for IgG anti- *Toxoplasma gondii* antibodies quantification, Talanta. 195 (2019) 699-705.

[16] M. Regiart, M. Rinaldi-Tosi, P.R. Aranda, F.A. Bertolino, J. Villarroel-Rocha, K. Sapag, G.A. Messina, J. Raba, M.A. Fernández-Baldo, Development of a nanostructured immunosensor for early and in situ detection of Xanthomonas arboricola in agricultural food production, Talanta. 175 (2017) 535-541.

[17] F.G. Ortega, M.A. Fernández-Baldo, M.J. Serrano, G.A. Messina, J.A. Lorente, J. Raba, Epithelial cancer biomarker EpCAM determination in peripheral blood samples using a microfluidic immunosensor based in silver nanoparticles as platform, Sens. Actuators. B. Chem. 221 (2015) 248-256.

[18] M. Regiart, M.A. Fernández-Baldo, J. Villarroel-Rocha, G.A. Messina, F.A. Bertolino, K. Sapag, A.T. Timperman, J. Raba, Microfluidic immunosensor based on mesoporous silica platform and CMK-3/poly-acrylamide-co-methacrylate of dihydrolipoic acid modified gold electrode for cancer biomarker detection, Anal. Chim. Acta. 963 (2017) 83-92.

[19] F. Tan, P.H.M. Leung, Z.B. Liu, Y. Zhang, L. Xiao, W. Ye, X. Zhang, L. Yi, M. Yang, A PDMS microfluidic impedance immunosensor for E. coli O157:H7 and Staphylococcus aureus detection via antibody-immobilized nanoporous membrane, Sens. Actuators. B. Chem. 159 (2011) 328-335.

[20] J. Casanova-Moreno, J. To, C.W.T. Yang, R.F.B. Turner, D. Bizzotto, K.C. Cheung, Fabricating devices with improved adhesion between PDMS and gold-patterned glass, Sens. Actuators. B. Chem. 246 (2017) 904-909.

[21] A. Waheed, M. Mansha, N. Ullah, Nanomaterials-based electrochemical detection of heavy metals in water: Current status, challenges and future direction, TrAC-Trend. Anal. Chem. 105 (2018) 37-51.

[22] L. Reverté, B. Prieto-Simón, M. Campàs**,** New advances in electrochemical biosensors for the detection of toxins: Nanomaterials, magnetic beads and microfluidics systems. A review, Anal. Chim. Acta. 908 (2016) 8-21.

[23] T. Hong, W. Liu, M. Li, C. Chen, Recent advances in the fabrication and application of nanomaterial-based enzymatic microsystems in chemical and biological sciences. Anal. Chim. Acta. 1067 (2019) 31-47.

[24] X. Wang, R. Niessner, D. Tang, D. Knopp, Nanoparticle-based immunosensors and immunoassays for aflatoxins. Anal. Chim. Acta. 912 (2016) 10-23.

[25] Z. Abed, J. Beik, S. Laurent, N. Eslahi, T. Khani, E.S. Davani, H. Ghaznavi, A. Shakeri- Zadeh, Iron oxide–gold core–shell nano-theranostic for magnetically targeted photothermal therapy under magnetic resonance imaging guidance, J. Cancer. Res. Clin. 145 (2019) 1213-1219.

[26] C. Karami, M.A. Taher, A catechol biosensor based on immobilizing laccase to Fe3O4@Au core-shell nanoparticles, Int. J. Biol. Macromol. 129 (2019) 84-90.

[27] E. Rasouli, W.J. Basirun, M.R. Johan, M. Rezayi, M. Darroudi, K. Shameli, Z. Shanavaz, O. Akbarzadeh, Z. Izadiyan, Facile and greener hydrothermal honey- based synthesis of Fe3O4/Au core/shell nanoparticles for drug delivery applications, J. Cell. Biochem. (2018) 1-8.

[28] S. Sabale, P. Kandesar, V. Jadhav, R. Komorek, R.K. Motkuri, X.Y. Yu, Recent development in synthesis, properties, and biomedical applications of core/shell

superparamagnetic iron oxide nanoparticles with gold, Biomater. Sci. 5 (2017) 2212-2225.

[29] S.V. Salihov, Y.A. Ivanenkov, S.P. Krechetov, M.S. Veselov, N.V. Sviridenkova, A.G. Savchenko, N.L. Klyachko, Y.I. Golovin, N.V. Chufarova, E.K. Beloglazkina, A.G. Majouga, Recent advances in the synthesis of Fe_3O_4@AUcore/shell nanoparticles, J. Magn. Magn. Mater. 394 (2015) 173-178.

[30] A. Sood, V. Arora, J. Shah, R.K. Kotnala, T.K. Jain, Multifunctional gold coated iron oxide core-shell nanoparticles stabilized using thiolated sodium alginate for biomedical applications. Materials Science and Engineering C 80 (2017) 274-281.

[31] Y. Yuan, S. Li, Y. Xue, J. Liang, L. Cui, Q. Li, S. Zhou, Y. Huang, G. Li, Y. Zhao, A Fe3O4@Au-basedpseudo-homogeneous electrochemical immunosensor for AFP measurement using AFP antibody-GNPs-HRP as detection probe, Anal. Biochem. 534 (2017) 56-63.

[32] J. Gao, X. Wang, Y. Zhang, J. Liu, Q. Lu, M. Chen, Y. Bai, Preparation and supercapacitive performance of nanosized manganese dioxide/ordered mesoporous carbon composites, Electrochim. Acta. 192 (2016) 234-242.

[33] R. Guo, L. Zhao, W. Yue, Assembly of core–shell structured porous carbon–graphene composites as anode materials for lithium-ion batteries, Electrochim. Acta. 152 (2015) 338-344.

[34] J. Hu, M. Noked, E. Gillette, Z. Gui, S. B. Lee, Capacitance behavior of ordered mesoporous carbon/Fe2O3 composites: Comparison between 1D cylindrical, 2D hexagonal, and 3D bicontinuous mesostructures, Carbon. 93 (2015) 903-914.

[35] R.J. Kalbasi, S.F. Rezayi, A novel bi-functional metal/solid acid catalyst for the direct reductive amination of nitroarenes synthesized on a resistant mesoporous carbon (CMK-8) support, J. Porous. Mat. 26 (2019) 641-654.

[36] T.N. Phan, M.K. Gong, R. Thangavel, Y.S. Lee, C.H. Ko, Enhanced electrochemical performance for EDLC using ordered mesoporous carbons (CMK-3 and CMK-8): Role of mesopores and mesopore structures, J. Alloy. Compd. 780 (2019) 90-97.

[37] T.N. Phan, M.K. Gong, R. Thangavel, Y.S. Lee, C.H. Ko, Ordered mesoporous carbon CMK-8 cathodes for high-power and long-cycle life sodium hybrid capacitors, J. Alloy. Compd. 743 (2018) 639-645.

[38] M. Regiart, J.L. Magallanes, D. Barrera, J. Villarroel-Rocha, K. Sapag, J. Raba, F.A. Bertolino, An ordered mesoporous carbon modified electrochemical sensor for solid-phase microextraction and determination of triclosan in environmental samples, Sensor. Actuat. B-Chem. 232 (2016) 765-772.

[39] Y.-R. Cui, C. Hong, Y.-L. Zhou, Y. Li, X.-M. Gao, X.-X. Zhang, Synthesis of orientedly bioconjugated core/shell Fe3O4@Au magnetic nanoparticles for cell separation, Talanta. 85 (2011) 1246-1252.

Figure captions

Scheme 1. Microfluidic device fabrication by photolithography.

Scheme 2. Analytical procedure for IgG anti-*T. canis* determination in human serum samples.

Figure 1. a) TEM image of CMK-8, b) N_2 adsorption-desorption isotherm at 77 K, and PSD (inset) of CMK-8, c) SEM micrograph of CMK-8-CH/GE, and d) EDS of CMK-8-CH/GE.

Figure 2. a) Cyclic voltammograms recorded in a 1 mmol L^{-1} $[Fe(CN)_6]^{3-/4-}$ in 0.1 mol L^{-1} KCl solution with a bare GE (b), and a CMK-8-CH/GE (c). Curve (a) corresponds to the CV recorded in the 0.1 mol L^{-1} KCl supporting electrolyte solution with the bare GE (Scan rate = 75 mV s^{-1}), b) EIS recorded in 5 mmol L^{-1} $[Fe(CN)_6]^{3-/4-}$ in 0.1 mol L^{-1} KCl, at 150 mV, varying the frequency with logarithmic spacing frequency in the range from 0.1 Hz to 100 kHz with bare GE, CH/GE, and CMK-8-CH/GE, and c) Cyclic voltammograms recorded in a 1 mmol L^{-1} $[Fe(CN)_6]^{3-/4-}$ in 0.1 mol L^{-1} KCl solution with the CMK-8-CH/GE at different scan rates (from a-h): 25, 50, 75 100, 125, 150, 175, 200 mV s^{-1}. The inset shows a plot of peak current values (Ip) as a function of the square root of the scan rate ($\nu^{1/2}$).

Figure 3. a) SEM micrograph of AuNPs@Fe_3O_4, and b) EDS of AuNPs@Fe_3O_4.

Figure 4. (a) Optimization of microfluidic device flow rate, (b) Optimization of pH enzymatic response, (c) Optimization of CMK-8 concentration employed for the electrode surface modification, and (d) Optimization of *T. canis* second-stage larvae (TES) antigens immobilization.

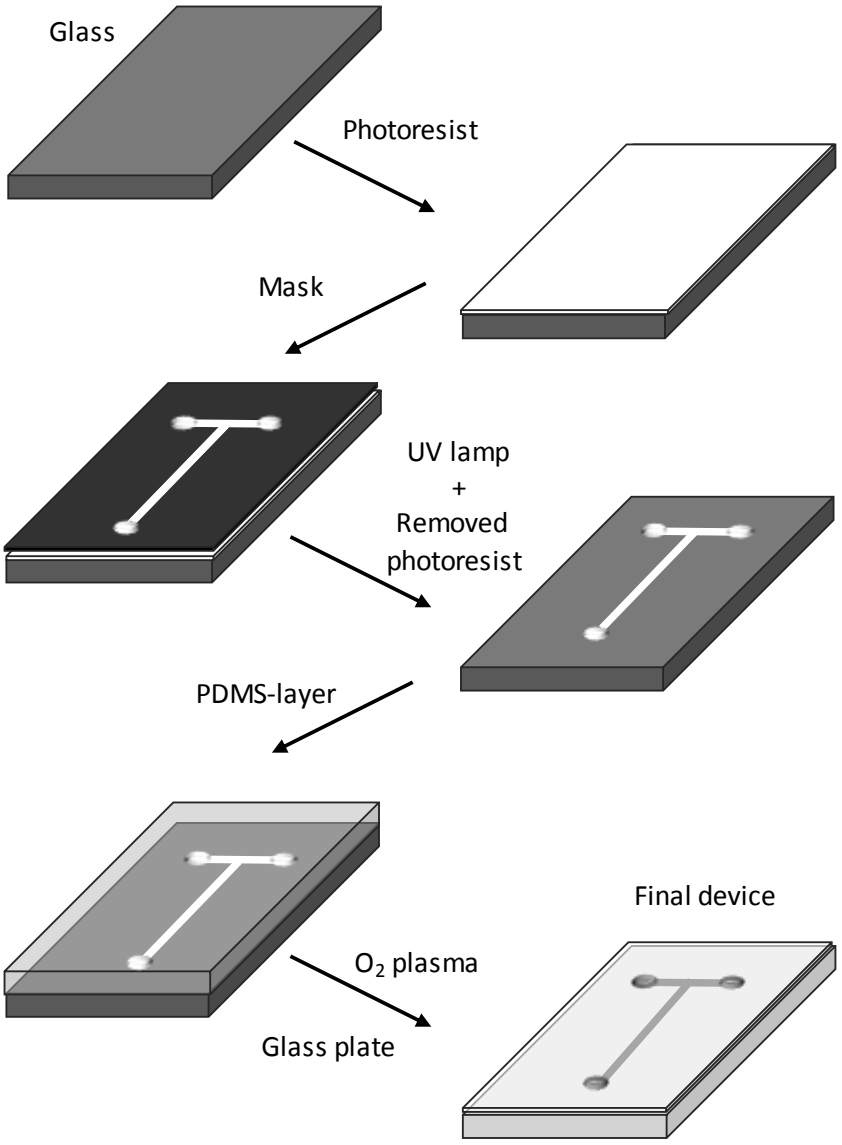
Glass
Photoresist
Mask
UV lamp
+
Removed
photoresist
PDMS-layer
Final device
O_2 plasma
Glass plate

Scheme 1

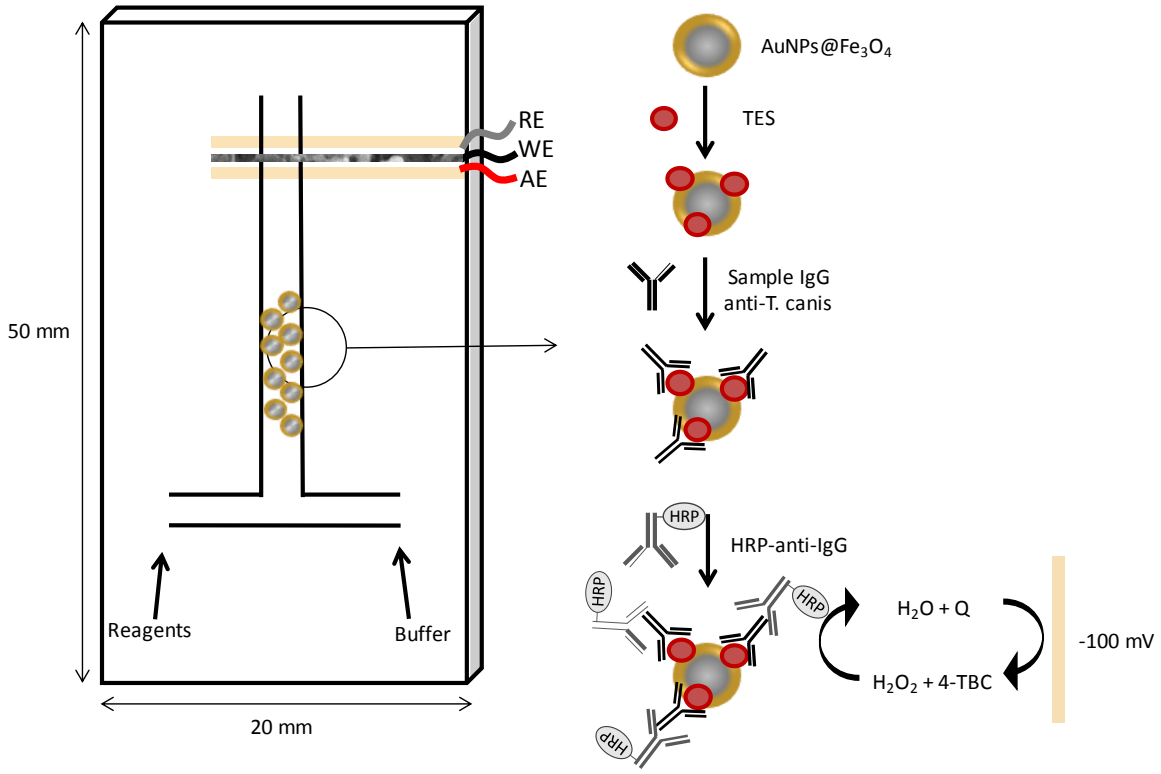
RE
WE
AE
50 mm
Reagents
Buffer
20 mm
AuNPs@Fe3O4
TES
Sample IgG
anti-T. canis
HRP
HRP-anti-IgG
H2O + Q
H2O2 + 4-TBC
-100 mV

Scheme 2

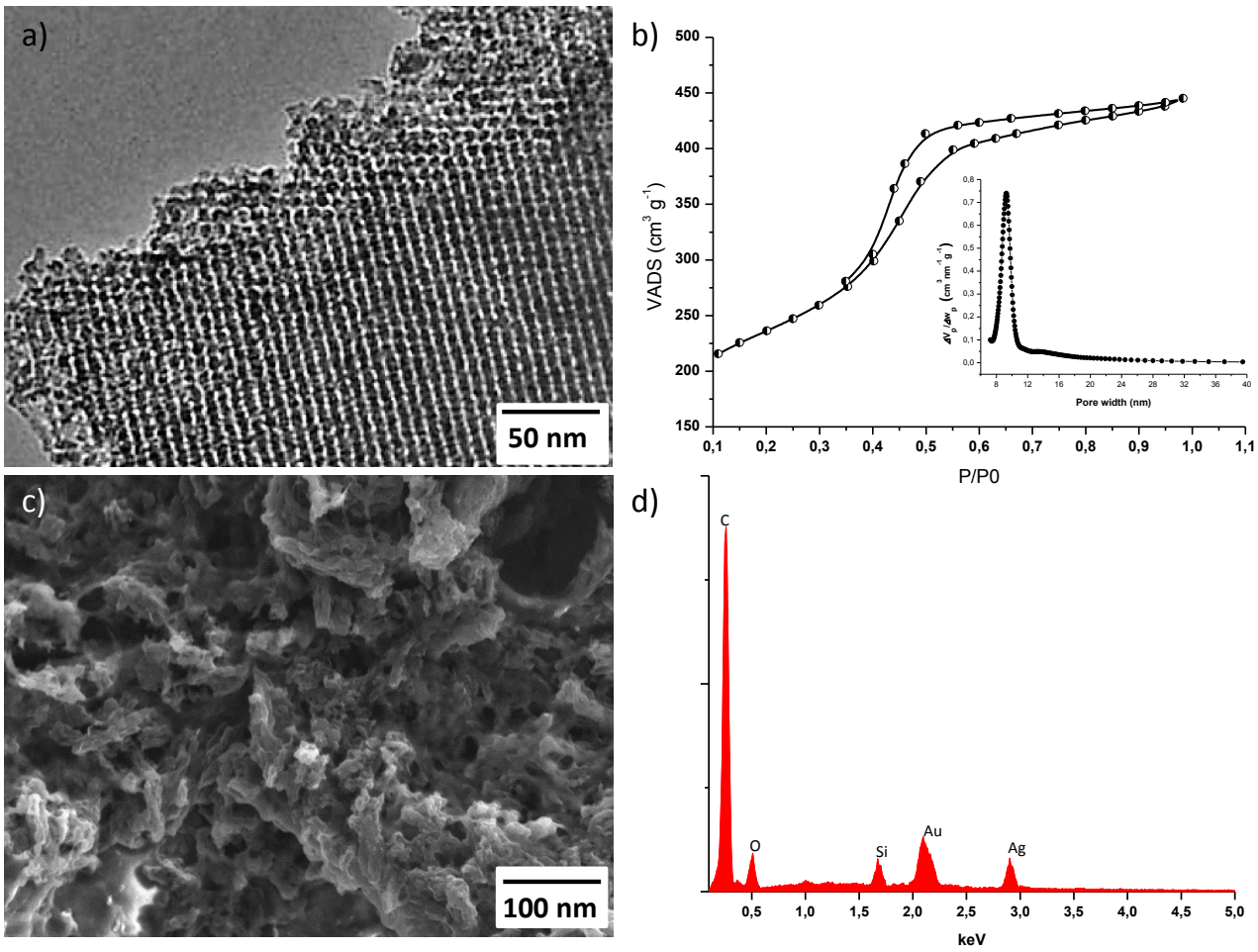

Figure 1

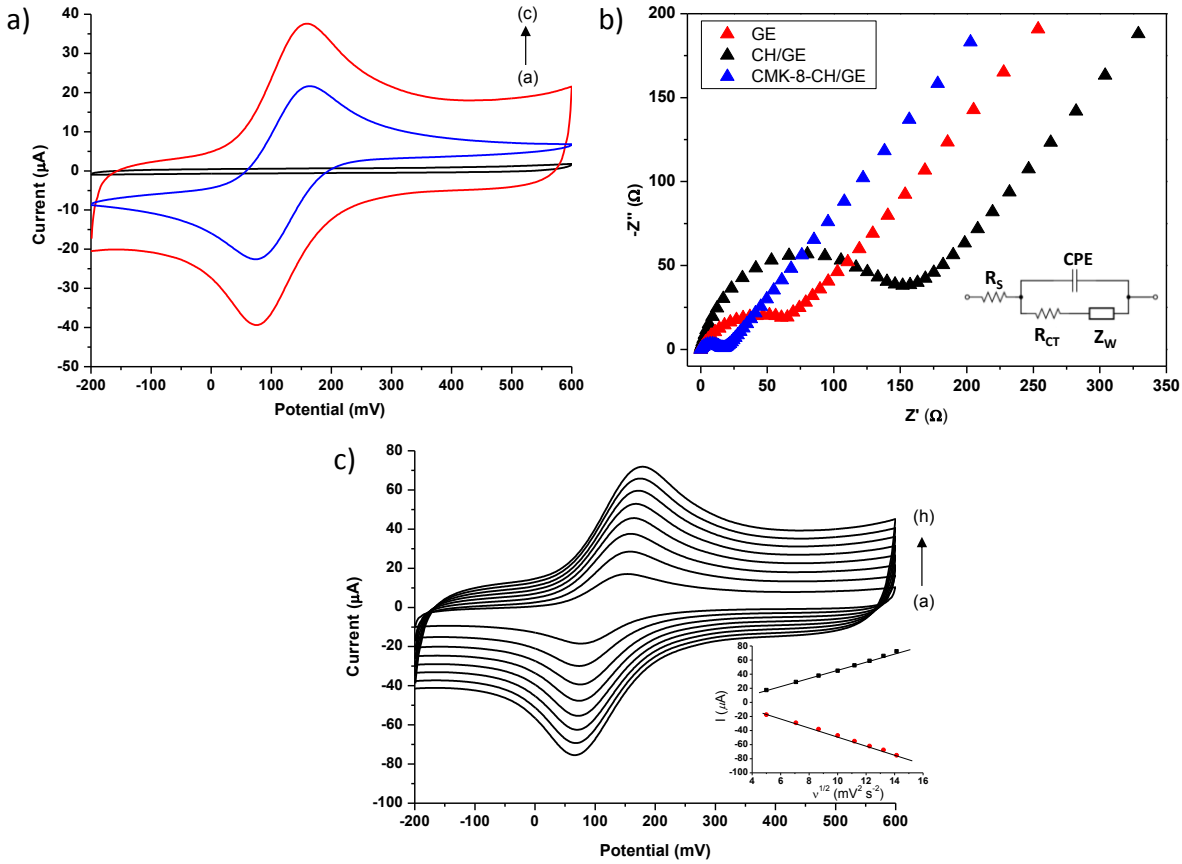
a)
(c)
(a)
Current (μA)
Potential (mV)
b)
GE
CH/GE
CMK-8-CH/GE
-Z'' (Ω)
Z' (Ω)
CPE
R_S
R_{CT}
Z_W
c)
(h)
(a)
Current (μA)
Potential (mV)
I (μA)
$v^{1/2}$ (mV^2 s^{-2})

Figure 2

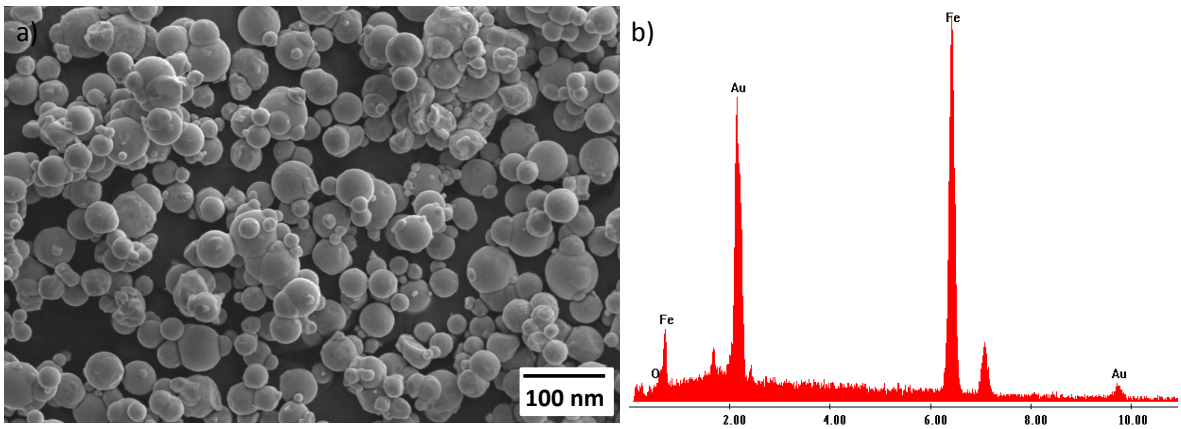

Figure 3

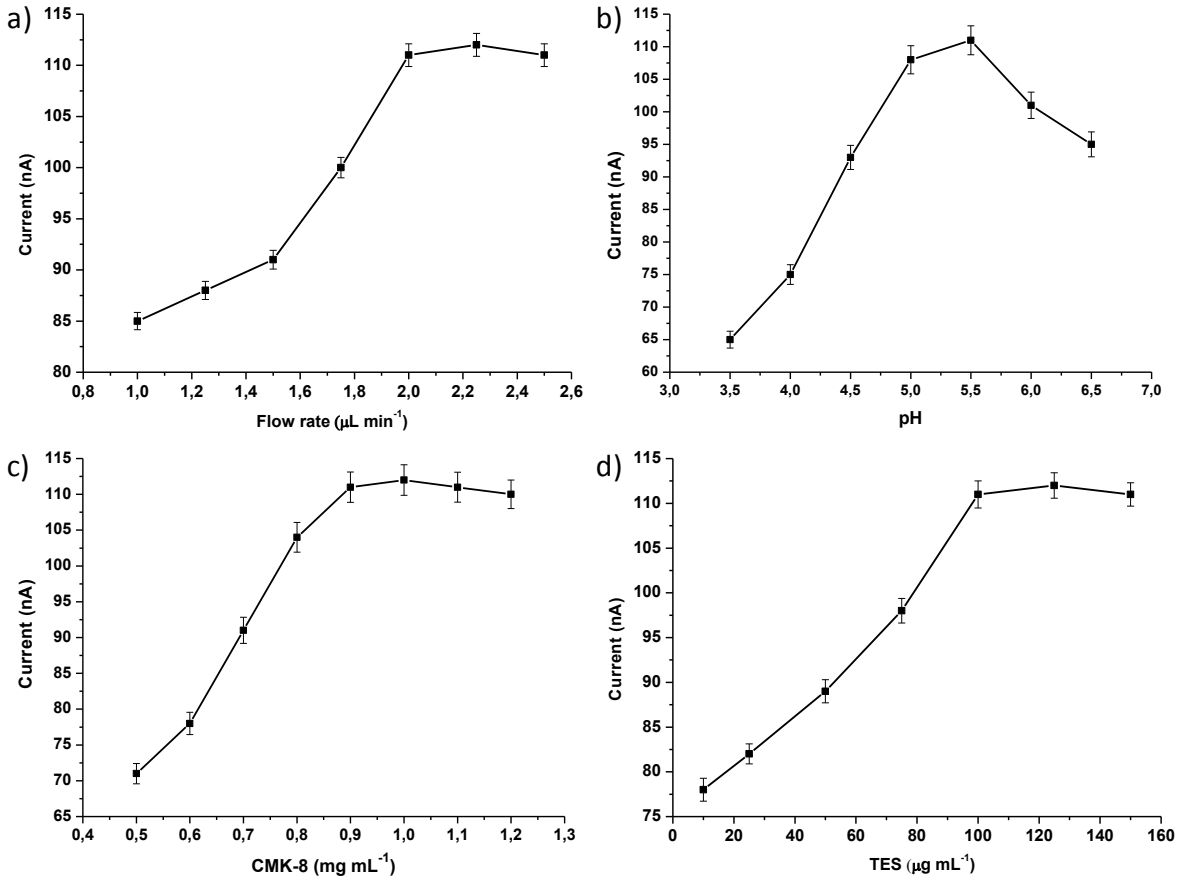
a)
Current (nA)
Flow rate (μL min-1)
b)
Current (nA)
pH
c)
Current (nA)
CMK-8 (mg mL-1)
d)
Current (nA)
TES (μg mL-1)

Figure 4

Table 1. Within-assay precision and between-assay precision for the microfluidic electrochemical immunosensor.

Samples[a]	Within-assay		Between-assay	
	Mean[b]	CV %	Mean	CV %
1	1.05	3.9	1.06	4.1
5	5.09	4.3	5.10	4.7
10	9.89	3.8	10.28	5.1
25	25.41	4.9	25.71	5.8
50	49.91	3.1	50.91	5.5
70	70.61	4.5	70.82	4.9

[a] Human serum samples ng mL^{-1} IgG anti-*T. canis* antibody.
[b] Mean of three determinations + S.D.

Table 2. Comparison of IgG anti-*T. canis* antibody concentration in human serum samples by microfluidic electrochemical immunosensor, microfluidic fluorescent immunosensor and ELISA.

Samples[a]	MEI[b]	MFI[c]	ELISA
1	1.05 + 0.01[d]	1.07 + 0.02	0.93 + 0.03
5	4.95 + 0.06	4.91 + 0.06	5.13 + 0.05
10	10.14 + 0.05	10.16 + 0.04	9.88 + 0.06
25	25.19 + 0.08	24.79 + 0.09	25.23 + 0.08
50	49.13 + 0.10	49.23 + 0.12	50.47 + 0.14
70	70.53 + 0.15	69.41 + 0.17	69.33 + 0.18

[a] Human serum samples ng mL^{-1} IgG anti-*T. canis* antibody.
[b] Microfluidic electrochemical immunosensor.
[c] Microfluidic fluorescent immunosensor.
[d] Mean of three determinations + S.D.

***Declaration of Interest Statement**

Declaration of interests

☒ The authors declare that they have no known competing financial interests or personal relationships that could have appeared to influence the work reported in this paper.

☐The authors declare the following financial interests/personal relationships which may be considered as potential competing interests: